Available online at www.sciencedirect.com
SCIENCE DIRECT®
International Journal of Heat and Fluid Flow 25 (2004) 373–383
International Journal of HEAT AND FLUID FLOW
www.elsevier.com/locate/ijhff

DNS of turbulent flow in a rod-roughened channel

Alireza Ashrafian [a], Helge I. Andersson [a,*], Michael Manhart [b]

[a] Department of Energy and Process Engineering, Norwegian University of Science and Technology, N-7491 Trondheim, Norway
[b] Fachgebiet Strömungsmechanik, Technische Universität München, D-85747 Garching, Germany

Abstract

A numerical investigation has been performed to study pressure-driven turbulent flow in a rod-roughened channel at Reynolds number $Re_\tau = 400$ based on the mean pressure-gradient. Both channel walls were roughened by square rods with a height k of only 1.7% of the channel height or $k^+ = 13.6$ in wall units. The pitch-to-height ratio was 8, which corresponds to the so-called "k-type" roughness and the resulting flow field was classified as "transitionally rough". The Reynolds-averaged streamline pattern exhibited two co-rotating vortices which filled the cavity between two consecutive rods. The averaged flow field which separated from one rod did not reattach and a return flow was observed all along the bottom of the cavity. Outside the roughness sublayer, i.e. beyond $5k$, no discernible streamwise variation of the mean velocity and second-order statistics could be observed, whereas the correlation between the streamwise and wall-normal mean velocity components persisted somewhat further away from the surface. Inside the roughness sublayer, however, significant differences in the turbulence field between smooth- and rough-wall layers were observed, for instance the high-energy region formed by the shear layer emanating from the crest of the roughness elements. Visualizations of instantaneous flow fields revealed the presence of elongated streaky structures similar to those routinely observed in flows along a smooth surface.

Keywords: Roughness; Turbulence; Channel flow; Square ribs

1. Introduction

Despite extensive studies of boundary layer flow on rough surfaces, the understanding of the physical mechanisms at work is still a subject of debate. The flow in the roughness sublayer is remarkably inhomogeneous and this is one reason why incomplete information is available from experimental studies of rough-wall boundary layers. Another difficulty in experiments is that the high turbulence intensities encountered near the roughness elements, cause many standard measurement techniques (X-wire anemometry in particular) to suffer from substantial errors that have often proven difficult to diagnose and correct (Raupach et al., 1991). Direct numerical simulation (DNS), on the other hand, allows the spatial and temporal evolution of the turbulent flow field to be examined in such detail that is not routinely available in a laboratory.

Rough-wall boundary layer research has been given significant attention in recent years. Measurements of several turbulence quantities and studies of coherent structures in turbulent boundary layers over rough walls have been carried out for instance by Wood and Antonia (1975), Bandyopadhyay (1987), Krogstad et al. (1992), Grass et al. (1993), Krogstad and Antonia (1999), Djenidi et al. (1999), Antonia and Krogstad (2001) and Bakken and Krogstad (2003). While the effects of surface roughness on the mean velocity profiles are now fairly well documented (e.g. Raupach et al., 1991 and Bergstrom et al., 2002), uncertainty still exists with respect to the effect a rough surface has on turbulent quantities (Krogstad and Antonia, 1999).

DNS, as well as large-eddy simulation (LES), has only recently been employed to examine turbulent flows over rough surfaces. From the perspective of the atmospheric boundary layer, Maass and Schumann (1994), De Angelis et al. (1997), Cherukat et al. (1998) and Henn and Sykes (1999) performed numerical simulations of turbulent flow in a channel with a sinusoidal bottom wall. Miyake et al. (2000) performed a DNS of turbulent flow and heat transfer in a plane channel with

* Corresponding author. Tel.: +47-73-59-35-56; fax: +47-73-59-34-91.
E-mail address: helge.i.andersson@ntnu.no (H.I. Andersson).

0142-727X/$ - see front matter © 2004 Elsevier Inc. All rights reserved.
doi:10.1016/j.ijheatfluidflow.2004.02.004

sand roughness on one wall. They continued their work by simulating a turbulent channel flow (Miyake et al., 2001 and Tsujimoto et al., 2001) in which the bottom wall was roughened by two-dimensional transverse square rods. The rod height, k, was 7% of the channel height. It was shown that the major effect of roughness was to enhance the turbulent mixing and heat exchange. Leonardi et al. (2003a,b) similarly performed DNS of fully developed channel flow with a rough bottom wall and smooth upper wall. The rough surface consisted of transverse square bars separated by a streamwise distance w. The height of the square bars was 10% of the channel height. A wide range of pitch to height ratio, λ/k, was considered. Here, λ denotes the pitch, i.e. the streamwise periodicity $w+k$ induced by the square rods. Very recently, DNS of one-sided rod-roughened channel flow has also been performed by Ikeda and Durbin (2002) and Nagano et al. (2003), whereas results of an LES were presented by Cui et al. (2003). A common feature of all these earlier computer simulations is that only one channel wall was roughened whereas the other wall remained smooth. The height of roughness elements was typically in between 5% and 10% of the channel height.

In the present work, DNS is employed for the first time to simulate turbulent flow in a channel with both walls roughened by square rods. The principal objective of the study is to investigate the roughness effects on the mean and turbulent flow fields and to examine how far from the near-wall region these effects are felt. To this end, we consider a roughness height k which is only 1.7% of the channel height. This relative roughness height is thus smaller than in all earlier simulations by at least a factor of 3.

2. Flow configuration

A sketch showing the channel, the flow orientation, the coordinate system, and the roughness shape is given in Fig. 1. A coordinate system is adopted in which x is aligned with the primary flow direction, y is measured vertically from the bottom wall, and z is parallel to the roughness crests. The domain size is $(L_x, L_y, L_z) = (6.528h, 2h, \pi h)$, i.e. practically the same as in the smooth channel simulation by Moser et al. (1999) at their intermediate Reynolds number (hereinafter denoted MKM395). The flow is statistically homogeneous in the spanwise direction. Periodic boundary conditions are used in the streamwise and spanwise directions and no-slip conditions are imposed at all rigid surfaces. The roughness elements are assumed to be two-dimensional, transverse square rods of cross section $k \times k$, positioned in a non-staggered arrangement on both walls (Fig. 1). The computational domain encompasses 24 square rods on each wall. The *pitch-to-height* ratio λ/k is 8, which is in the range that Furuya et al. (1976) found to exhibit the largest influence on the mean velocity profile. Perry et al. (1969) called this type of roughness configuration "k-type roughness" since the roughness function showed a clear dependency on k. The roughness height is 1.7% of channel height ($k = 0.034h$) which amounts to 13.6 times the viscous length scale v/u_τ. Here, u_τ is defined as $u_\tau \equiv \left(-\frac{h}{\rho}\frac{\mathrm{d}P}{\mathrm{d}x}\right)^{1/2}$, where ρ is the fluid density and $\mathrm{d}P/\mathrm{d}x$ is the imposed pressure gradient. According to the classification suggested by Ligrani and Moffat (1986), the flow regime is thus transitionally rough, i.e. the flow depends both on the Reynolds number and the roughness height.

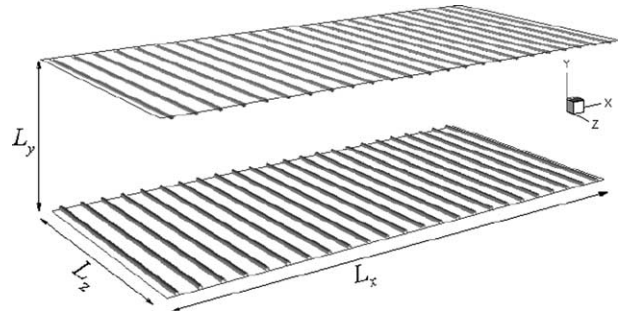

Fig. 1. Schematic of the flow configuration.

3. Numerical method and resolution

The governing equations for an incompressible Newtonian fluid, i.e. the Navier–Stokes equation and the continuity equation, are integrated over a finite volume according to the *volume-balance method* of Schumann (1975). The resulting equations are solved numerically on a staggered and non-uniform Cartesian grid by the parallel computer code MGLET (Manhart, 2004). Pressure is defined at the center of each grid cell and the velocity components at the interfaces. Velocity components and their derivatives are obtained by linear interpolation and central differences respectively. As a result, the spatial discretisation is of second-order accuracy. Using a leapfrog scheme for the explicit time integration of the momentum equations, a second-order accurate time step is achieved. This combination of central differencing and a leapfrog time step is energy conserving for the one-dimensional convection equation and therefore appropriate for DNS. The Poisson equation for the pressure is solved by a multi-grid method based on pointwise velocity–pressure iterations. The computational grid is divided into an arbitrary number of subgrids that are treated as independent grid blocks in parallel processing. MGLET is a block-structured code in order to manage multiple grids that arise from the parallelization (see Manhart et al., 2001 for more details). Validation of

the simulation code has been performed in the course of various DNS and LES studies of turbulent flow in a smooth channel (Manhart et al., 1998), and separating and reattaching turbulent boundary layer flow (Manhart and Friedrich, 2002).

A constant mean pressure-gradient $dP/dx < 0$ drives the flow throughout the rod-roughened channel. The driving pressure gradient is fixed such as to achieve a friction Reynolds number $Re_\tau \equiv u_\tau h/\nu$ equal to 400, i.e. essentially the same as the intermediate Reynolds number case reported by MKM395. Uniform grid spacing is selected for the streamwise and spanwise directions. A total of 768 computational cells are used in the x-direction and 160 cells in the z-direction. In the wall-normal direction, the total number of computational cells is 160, out of which 24 are equally placed within the distance $y = 3k$ from the channel walls so that the minimum grid spacing is $\Delta^+_{y\min} = 1.7$. Accordingly, the first grid point at which the streamwise velocity is computed is located at $y_1^+ = 0.85$. The grid resolutions in the two homogeneous directions are $\Delta_x^+ \approx 3.2$ and $\Delta_z^+ \equiv 7.85$ in wall units. With this resolution, three nodes are embedded in the viscous sublayer, i.e. inside of $y^+ = 5$.

In previous LES investigations of turbulent flow over obstacles with sharp edges (Werner and Wengle, 1993), spurious oscillatory modes (“wiggles”) have been observed upstream of the leading edge where the velocity gradients are steep. These “wiggles” come from the insufficient properties of the second-order central approximations used. In the present simulation, the fine spatial resolution was sufficient to hold the cell-Peclet number in the range of two where wiggles cannot be observed any more.

4. Results

The direct outcome of a DNS is the time-dependent and three-dimensional fields for the three velocity components (U: streamwise, V: wall-normal and W: spanwise) and the pressure P. Statistical averaging (denoted by $\langle\rangle$) is performed in the homogeneous spanwise direction and time so that single-point statistics are functions of both x and y. Statistics are collected over approximately 40 nearly independent data fields, all separated by $0.5t^*$, where t^* is the time unit h/u_τ. For the fully developed flow, the mean quantities vary periodically with a periodicity equal to the roughness pitch (λ) that implies a quasi-homogeneity in the streamwise direction. The points (x, y) and $(x + n\lambda, y)$, where n is an integer, are statistically equivalent and the number of samples are substantially increased by taking advantage of this streamwise periodicity. Results are reported at the four characteristic streamwise positions shown in Fig. 2.

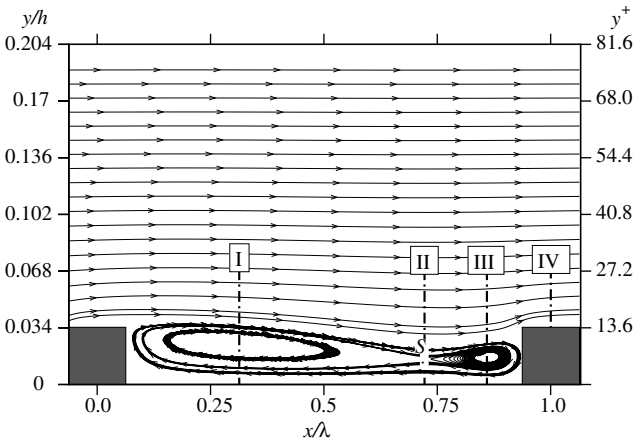

Fig. 2. Streamline pattern in the vicinity of the roughness elements. The Roman numerals identify chosen streamwise locations.

4.1. Mean velocity

The streamlines associated with the statistically averaged mean flow $\langle U\rangle$ and $\langle V\rangle$ are shown in Fig. 2. A modest expansion of the core flow can be observed above the cavity formed by two consecutive rods, whereas the streamlines beyond $y/h \approx 0.1$, i.e. more than three rod heights k from the surface, are practically parallel. Two recirculation zones fill most of the cavity. The mean flow separates from the roughness elements and forms a large separation bubble downstream of each rod, whereas a smaller vortex with the same sign of circulation is formed just upstream of the next rod. The mean flow does never attach at the bottom of the cavity, but instead forms a saddle point (S) in between the two recirculation zones. Leonardi et al. (2003b), at exactly the same pitch-to-height ratio but significantly higher k^+, observed that the flow reattached to the bottom and formed a short recovery region before another flow separation occurred. In the present case, however, the absence of a reattachment point at the cavity bottom gives rise to a continuous return flow all along the bottom surface. The resulting wall shear stress is therefore acting in the direction of the core flow.

The reason why the flow does not reattach in the present case can be described to the significantly lower turbulence intensities, and thus a correspondingly low turbulent diffusivity, downstream of the trailing corner of a roughness element, as will be shown in 4.4. Here, it should be recalled that the height of the rods is $k^+ = 13.6$ (measured in wall units), whereas Leonardi et al. (2003b) simulated a flow with k^+ about 90, i.e. more than six times larger rods.

Fig. 2 indicates some selected locations I–IV. Section I is located at the focal point of the primary recirculation zone downstream of the roughness element ($x/\lambda = 0.312$). Section II is located at the saddle-point

between the two recirculation zones ($x/\lambda = 0.71$) and Section III is located at the focal point of the second recirculation zone ($x/\lambda = 0.875$). Finally, Section IV is located at the center of the roughness crest ($x/\lambda = 1.0$).

The mean velocity profile with some different scalings is compared to the smooth case in Fig. 3. For the rough case, the streamwise velocity $\langle U \rangle$ at $x/\lambda = 0.312$ is reported. Velocity profiles at other streamwise locations collapse in the outer region. The rough-wall profile in outer coordinates in Fig. 3(a) shows a significant deviation from the smooth case all across the channel. Owing to the higher surface drag, the flow rate is reduced and the mean velocity profile on the rough surface is less bodied than that obtained on a smooth surface. In the outer region the mean velocity defect can be expressed as $(U_0 - \langle U \rangle)/u_\tau = f(y/h)$ where U_0 is the center-line velocity. As can be seen from Fig. 3(b) the profiles collapse in the outer region. This observation suggests that $f(y/h)$ is universal, i.e., the velocity characteristics are independent of surface geometry in the outer region. This is indeed consistent with Townsend's (1976) Reynolds number similarity hypothesis. Fig. 3(c) shows the defect profiles scaled with center-line velocity U_0, which is similar to the scaling George and Castillo (1997) proposed for smooth-wall zero pressure-gradient boundary layers. In presence of roughness, the defect profile shifts upwards. Velocity profiles normalized by u_τ are shown in Fig. 3(d). For a given pressure-gradient, the average velocity $\langle U \rangle$ decreases, as expected. The log-region is preserved and shifted downwards in accordance with the *law-of-the-wall*

$$U^+ = \frac{1}{\kappa} \ln y^+ + B - \Delta U^+, \tag{1}$$

where κ is the von Kármán constant. ΔU^+ is called the *roughness function* and is a measure of the capacity of the surface to absorb momentum or, in other words, is a measure of the increase in local drag due to roughness. In fully rough flows the roughness function is known to vary logarithmically with k^+, i.e. in accordance with $\Delta U^+ = \frac{1}{\kappa} \ln k^+ + C$, where $C = 1.2$ in boundary layer flows (Krogstad and Antonia, 1999) and 1.9 in rod-roughened channel flow (Bakken and Krogstad, 2003). The downward shift ΔU^+ is about 7.0 in Fig. 3(d), whereas the curve-fit formula due to Bakken and Krogstad gives $\Delta U^+ \approx 8.3$. The observation that ΔU^+ is significantly below the experimentally deduced relationship for the fully rough flow regime suggests that the present flow is transitionally rough. The much higher value $\Delta U^+ \approx 13.2$ found by Leonardi et al. (2003b) for the same pitch-to-height ratio is consistent with their six times larger value of k^+ and, moreover, quite close to the experimentally observed logarithmic variation.

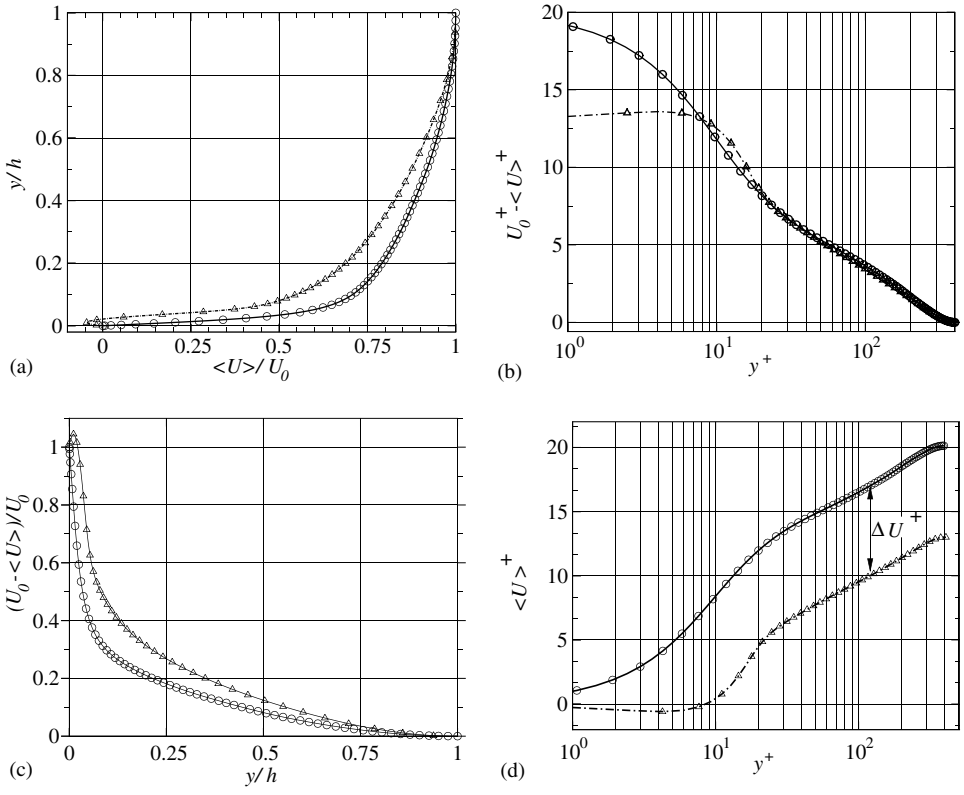

Fig. 3. Mean velocity profile at $x/\lambda = 0.312$. Circles represent smooth channel data due to MKM395: (a) outer scaling; (b) defect law, inner scaling; (c) defect law, outer scaling and (d) inner scaling.

4.2. Momentum balance

In flows over rough surfaces, the roughness elements distort the streamwise mean flow in the near-wall region, as indicated already by the bulging of the streamlines depicted in Fig. 2. The contour plot of the mean wall-normal velocity component in Fig. 4(a) shows periodically alternating flows towards the wall and away from the wall in the near-wall region. The streamwise momentum equation for the rough-wall channel flow can be written as

$$0 = -\frac{\partial\langle P\rangle}{\partial x} + \frac{\partial}{\partial x}\left(\mu\frac{\partial\langle U\rangle}{\partial x} - \rho\langle u^2\rangle - \rho\langle U\rangle^2\right) + \frac{\partial}{\partial y}\left(\mu\frac{\partial\langle U\rangle}{\partial y} - \rho\langle uv\rangle - \rho\langle U\rangle\langle V\rangle\right). \quad (2)$$

It can be seen from the RHS of Eq. (2) that there is a contribution of mean momentum transport $-\rho\langle U\rangle\langle V\rangle$ to the shear stress. This contribution is absent in case of a smooth-wall channel flow where $\langle V\rangle$ is everywhere zero. Contours of $-\langle U\rangle\langle V\rangle$ are shown in Fig. 4(b) and reveal large positive pockets midway between the crests of two neighboring rods. Fig. 5 shows the variation of $-\langle U\rangle\langle V\rangle$ and the viscous and turbulent terms across the channel over the roughness crest. $-\langle U\rangle\langle V\rangle$ is maximum at $y/h \approx 0.05$. Moreover, $\langle U\rangle$ and $\langle V\rangle$ become uncorrelated at a vertical distance from the boundary larger than $y/h \approx 0.35$ or about $10k$. The rod-induced correlation $\langle U\rangle\langle V\rangle$ is of dynamical importance in the immediate vicinity of the rods, where its magnitude exceeds $2u_\tau^2$. At a distance $5k$ away from the surface, however. $\langle U\rangle\langle V\rangle$ has been reduced by a factor 20, which makes its contribution to the total shear in Eq. (2) of marginal importance.

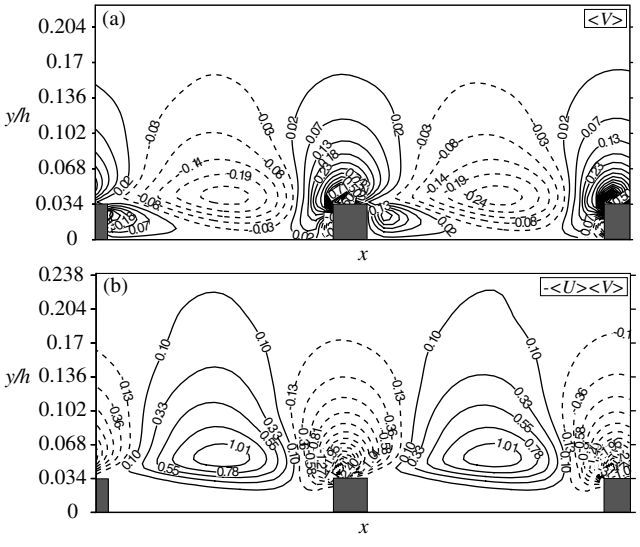

Fig. 4. (a) Contours of $\langle V\rangle$ normalized by u_τ, (b) contours of $-\langle U\rangle\langle V\rangle$ normalized by u_τ^2.

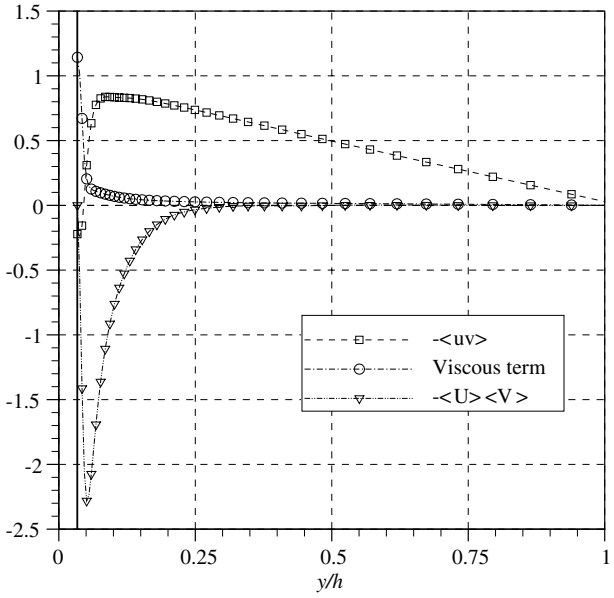

Fig. 5. Variation of contributions to the apparent shear stress across the channel at $x/\lambda = 1.0$. Each term is normalized by u_τ^2.

At $y/h \approx 0.05$, $\overline{\langle U\rangle\langle V\rangle}$ is about $0.08\overline{\langle uv\rangle}$, where the over bar denotes averaging over one roughness period λ. Djenidi et al. (1999), who studied a turbulent boundary layer over a d-type roughness, estimated on the basis of their LDV measurements $\overline{\langle U\rangle\langle V\rangle}$ to be about $0.33\overline{\langle uv\rangle}$ in the plane of roughness crests, i.e. significantly more influential than in the present case.

4.3. Friction and form drags

In a smooth channel, like that considered by MKM395 and others, the driving pressure gradient $\mathrm{d}P/\mathrm{d}x$ is required to overcome the wall shear stress τ_w. In a rod-roughened channel, however, both form drag and skin friction contribute to the flow resistance. Since the mean flow varies periodically with x in the present configuration, so does τ_w. Let us now define a local skin-friction coefficient $C_f(x) \equiv \tau_w(x)/(\frac{1}{2}\rho U_0^2)$ where U_0 denotes the centerline velocity. Here, $\tau_w(x)$ is evaluated along the bottom of the cavities and along the crest of the rods. The streamwise variation of the skin-friction is presented in Fig. 6. A high level of C_f is observed at the leading corner of the rod and the wall-friction therefore decays with x, similarly to the decaying C_f in a turbulent boundary layer at a flat plate. Here, C_f remains positive all along the crest, whereas Leonardi et al. (2003b) observed flow separation, i.e. $C_f < 0$, for $\lambda/k > 8$ in their parameter study. All along the bottom of the cavity formed by two consecutive rods, however, C_f is negative, as expected in view of the streamline pattern displayed in Fig. 2. The streamwise-averaged skin friction $\overline{C_f} = 4.5 \times 10^{-4}$. In the rod-roughened channel, the difference ΔP between the surface-averaged pressure on

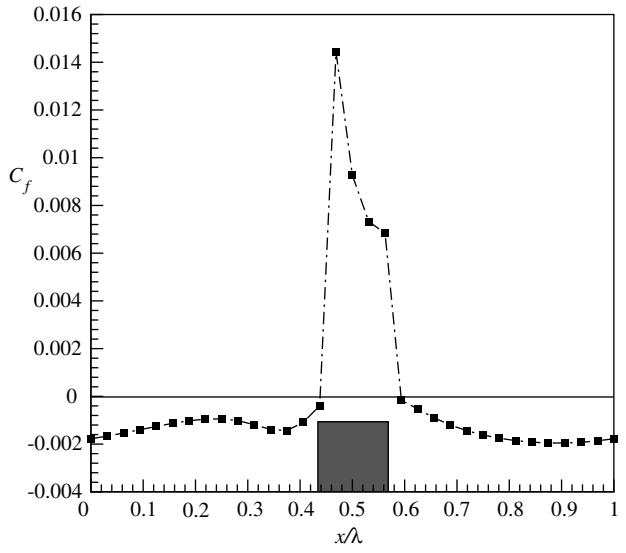

Fig. 6. The streamwise variation of the skin-friction coefficient C_f.

the leading and trailing surfaces of the rods causes the form drag, which can be expressed in terms of a dimensionless drag coefficient $C_d \equiv \Delta P/(\frac{1}{2}\rho U_0^2)$. In the present case C_d is obtained to be 9.2×10^{-2} and this form drag is responsible for the entire flow resistance, except that exerted by the crest of the rods.

4.4. Turbulence statistics

Significant distortions in the turbulent stress fields arc generated by the roughness elements. Contour plots in Fig. 7 show the variation of Reynolds stresses in the xy-plane. The horizontal dashed-line in the plots indicates the estimated thickness of the roughness sublayer, i.e. 5 times the roughness height, according to Townsend (1976). It is seen that the inhomogeneity in turbulence stresses does not extend beyond $y/h \approx 0.17$ ($y^+ \approx 68$) and the roughness effects are apparently felt only inside the roughness sublayer. The streamwise normal stress $\langle u^2\rangle$ attains its maximum over the cavity region, while the spanwise component (w^2) exhibits a peak level just upstream of the rods' leading edges. The turbulent intensities are significantly lower downstream of the trailing edge of the roughness elements. The greatest contribution to the Reynolds shear stress comes from the region above the saddle point, i.e. somewhat upstream of the leading edge of the roughness elements. Comparison between the contour plots of $-\langle uv\rangle$ in Fig. 7 and contours of mean wall-normal velocity, $\langle V\rangle$, in Fig. 4(a) shows that the regions of high Reynolds shear stress corresponds to the regions in which $\langle V\rangle$ changes sign.

The variation of the normalized Reynolds stresses from the wall to the centerline is shown in Fig. 8 in outer coordinates and in Fig. 9 in inner coordinates. The vertical dashed line indicates the estimated thickness of the roughness sublayer. Inside this layer, the maximum value of the streamwise Reynolds stress is significantly reduced as it depicts the direct effect of the presence of the roughness elements. Outside the roughness sublayer, however, the profiles of the individual Reynolds stress components became independent of the streamwise

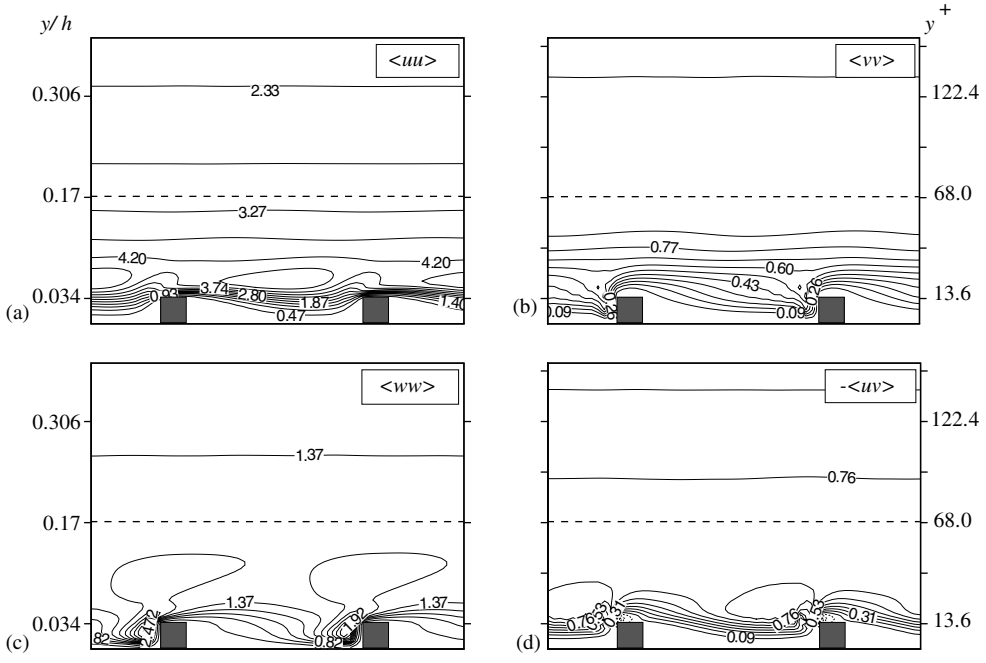

Fig. 7. Contours of Reynolds stresses normalized by u_τ^2.

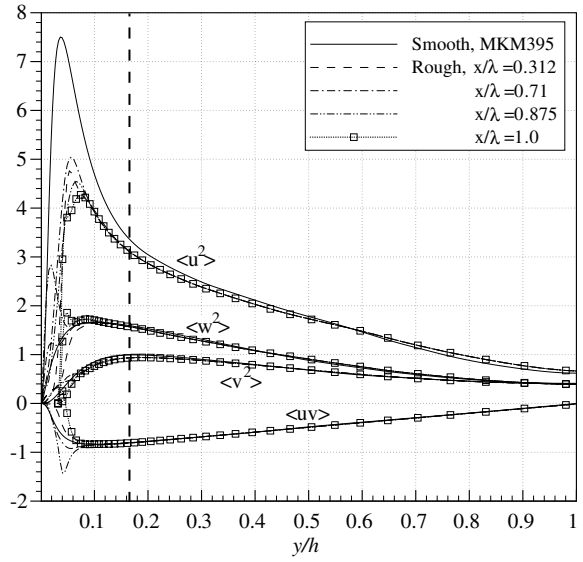

Fig. 8. Reynolds stresses in outer coordinates, normalized by u_τ^2.

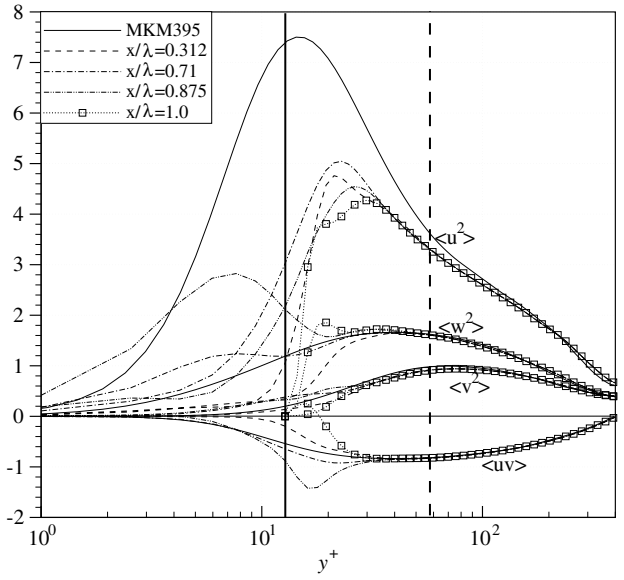

Fig. 9. Reynolds stresses in inner coordinates, normalized by u_τ^2.

location x/λ. Moreover, the variation with y is about the same as in smooth channel flow (MKM395).

Fig. 9 in which the vertical solid line indicates the location of the crest of the roughness elements, highlights the near-wall region. The largest turbulent stresses are generated in layers above the plane of the roughness crests, whereas at the crest plane the turbulence level is rather low. Most noticeable is the distinct peak in the spanwise Reynolds stress at $x/\lambda = 0.875$. This is believed to be due to the blocking effect of the roughness elements. The energy is removed from the streamwise component and redistributed among the spanwise and wall-normal stresses. A tiny region near the crest of the rod can also be observed, in which the off-diagonal component $\langle uv\rangle$ becomes positive, cf. the profile of $\langle uv\rangle$ at $x/\lambda = 1.0$ in Fig. 9.

4.5. Production of the turbulent kinetic energy

The time-averaged mean rate of production of turbulent kinetic energy (TKE), $\mathscr{P}$, is given by the following equation:

$$\mathscr{P} \equiv -\langle uv\rangle \frac{\partial\langle U\rangle}{\partial y} - \langle u^2\rangle \frac{\partial\langle U\rangle}{\partial x} - \langle uv\rangle \frac{\partial\langle V\rangle}{\partial x} - \langle v^2\rangle \frac{\partial\langle V\rangle}{\partial y}. \tag{3}$$

Here, the turbulent kinetic energy per unit mass is defined as $(\langle u^2\rangle + \langle v^2\rangle + \langle w^2\rangle)/2$. The first two terms on RHS of Eq. (3) represent a direct transfer of energy from the mean flow to the streamwise contribution $\langle u^2\rangle/2$. The third and fourth terms represent a direct transfer to $\langle v^2\rangle/2$. The last three terms in Eq. (3) vanish identically in a smooth channel whereas in the rough case, these terms can obtain significant values in localized areas close to the roughness elements. The first term, however, is dominant throughout most of the two-dimensional field. The TKE production $\mathscr{P}$ in Eq. (3) is computed from the simulated flow field and made dimensionless with u_τ^4/ν. The contours in Fig. 10 exhibit a wide production maximum somewhat upstream of the rods and flush with their crests. Inside the cavity and near the bottom-wall, the production rate is rather small. Fig. 11 depicts the profiles of TKE production at various streamwise locations. The values of the rough-wall TKE production within the roughness sublayer region are higher than in the smooth case, except in the innermost wall-region, i.e. $y < k$.

Above the crest of the rods, the TKE production exhibits an exceptional variation. The abrupt drop in the Reynolds shear stress $-\langle uv\rangle$ below $y^+ = 30$ (see Fig. 9) makes the primary production unusually small in this particular area. The alternating sign of $\mathscr{P}$ is associated

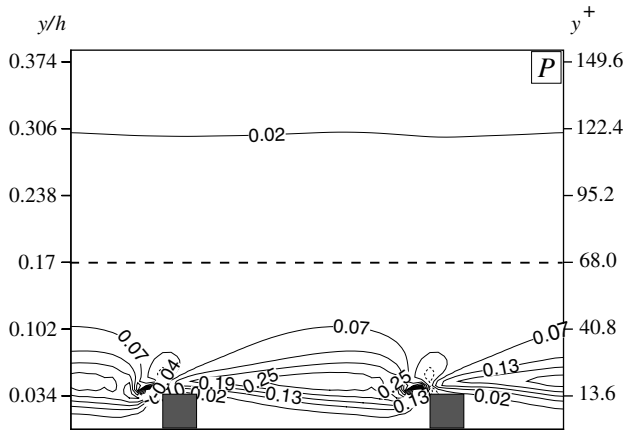

Fig. 10. Turbulent kinetic energy production normalized by u_τ^4/ν.

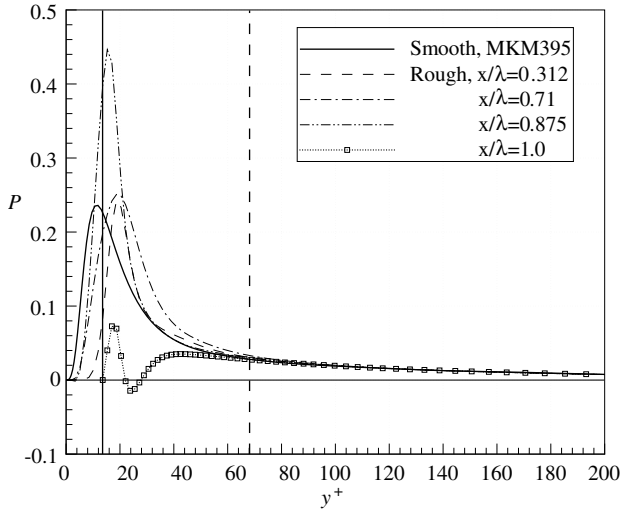

Fig. 11. Variation of the turbulent kinetic energy production normalized by u_τ^4/ν.

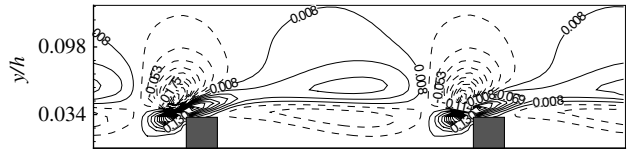

Fig. 12. The secondary production term $-\langle u^2\rangle \frac{\partial\langle U\rangle}{\partial x}$ normalized by u_τ^4/ν.

with the variation of the secondary production term on the RHS of Eq. (3), as presented in Fig. 12. In the immediate vicinity of the crest of the rods, the flow is decelerated and $-\langle u^2\rangle \frac{\partial\langle U\rangle}{\partial x}$ becomes positive, whereas a flow acceleration takes place a little further away from the leading edge of the rods where $-\langle u^2\rangle \frac{\partial\langle U\rangle}{\partial x} < 0$. The secondary production term thus tends to enhance the TKE very close to the roughness crest and reduce it further out. This observation suggests that the TKE-producing structures are locally quenched by the crest of the roughness elements. Outside the roughness sublayer, on the other hand, the value of TKE production is same as in the smooth case. This is another evidence that the effects of roughness on the turbulence field are rather confined to the roughness sublayer.

4.6. Instantaneous turbulence characteristics

Previous studies of the smooth-wall turbulence have shown that the coherent quasi-streamwise vortical structures are responsible for TKE production peak in the near-wall region (e.g. see Kline and Robinson, 1990). However, it is not unlikely that different flow structures may contribute to the TKE production over the rough surface. As it can be seen from Fig. 10, the production of TKE on the rough surface is associated with the shear layer emanating from the crest of the roughness elements. The study of the structure of turbulence in the roughness sublayer may thus provide an answer to the question whether or not the TKE-producing structures in the rough-wall turbulence are similar to those near a smooth wall.

To this end, contours of the instantaneous fluctuating part of the streamwise and spanwise components of the velocity (u and w) in different xz-planes are shown in Fig. 13. Close to the bottom wall and within the cavity valley at $y^+ = 6$, the low momentum fluid is trapped between the roughness elements and no coherent structures can practically be formed in the streamwise direction (Fig. 13(a)). Instead, small organized pockets of positive and negative fluctuating velocity in the spanwise direction can be observed (Fig. 13(b)). In the immediate vicinity of the crest of the roughness elements and in the plane located at vertical position $y^+ = 14$, some structures are formed just above the cavity region (Fig. 13(c)). Darker areas represent the low-speed fluid. These structures are locally interrupted by the roughness elements. However, the coherence of the structures persists over successive roughness elements and resembles the streaky pattern which can be seen in Fig. 13(e) at $y^+ = 20$. At this wall distance, which coincides with the peak of the TKE production in Figs. 10 and 11, some streaky structures elongated in the streamwise direction are present. Their organization, however, is distorted by the high turbulence intensities present in the field. This is evident from Fig. 13(c), (d) and (f) where no obvious coherence is seen in the spanwise fluctuation, Leonardi et al. (2003a) observed elongated near-wall structures for flow over square cavity ($\lambda/k = 2.0$), but streaky flow patterns like those in Fig. 13(e), could not be discerned for the pitch-to-height ratio $\lambda/k = 8.0$. Since no streaky structures are present in fully rough flow past a k-type surface, the presence of streaks in the present case is another indication that the flow is transitionally rough.

In order to portray the instantaneous flow structures in the rough-wall channel flow, the objective detection criterion of Jeong and Hussain (1995) is employed. They found that true vortical structures buried within a shear layer are well-presented by connected regions where the second largest eigen-value (λ_2) of the tensor $S_{ik}S_{kj} + \Omega_{ik}\Omega_{kj}$ is negative. S_{ij} and Ω_{ij} are the symmetric and anti-symmetric parts of the velocity gradient tensor $u_{i,j} = \partial u_i/\partial x_j$, respectively. The λ_2-based vortex definition is powerful enough to extract organized events from the background shear characteristic of boundary layers. Since λ_2 values are Galilean invariant, they are reliable indicators of coherent vortex structures. The vortical structures are extracted by plotting iso-surfaces of λ_2 (normalized by u_τ^4/ν^2) equal to some threshold. Snapshots of vortical structures with threshold of 3.8% of the maximum value of −0.55 are shown in Fig. 14(a) and

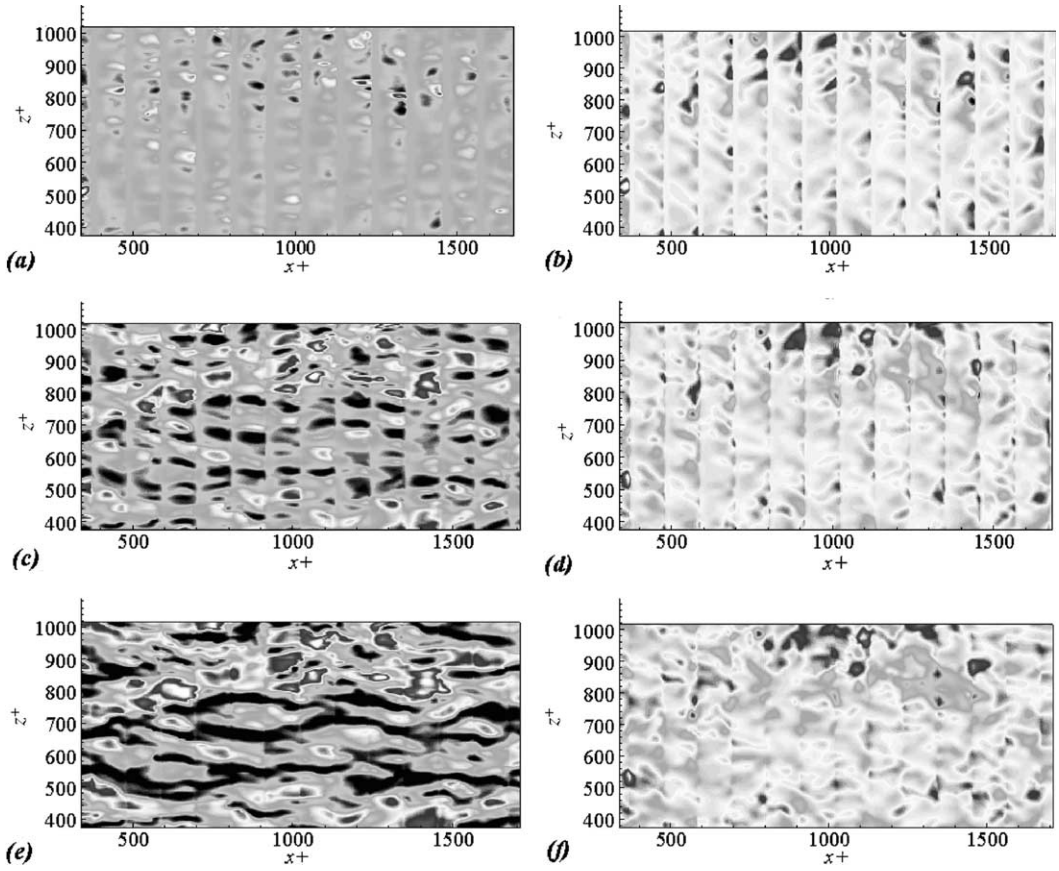

Fig. 13. Iso-surfaces of the fluctuating velocity in the streamwise (left panel) and spanwise (right panel) directions: (a) and (b) $y^+ = 6$; (c) and (d) $y^+ = 14$; (e) and (f) $y^+ = 20$.

(b), for the rough-wall and smooth-wall channels. The present choice was made so that the various vortical structures would be easily identifiable with minimal background noise.

Fig. 14 shows that various vortical structures are densely populated in the boundary layer over the rough surface. In the smooth case, the majority of the vortical structures are aligned in the streamwise direction whereas in the rough case, rather complex patterns of vortical structures are observed. Some quasi-streamwise structures with less organization in the spanwise direction are formed within the roughness sublayer. Incoherent spanwise vortical structures are shed from the crest of the roughness elements and consequently, a high degree of three-dimensionality of the flow is observed in the vicinity of the two-dimensional roughness elements. This is a remarkable feature of the turbulence production in the roughness sublayer. The quasi-streamwise vortices formed in the roughness sublayer are disrupted by colliding into either roughness elements or other vortical structures shed from the roughness elements and therefore, as a result of such a complex mechanism, a high-energy layer is formed above the plane of the roughness crests.

5. Concluding remarks

The present paper provides results from a direct numerical simulation of pressure-driven flow in a plane channel. Unlike all other computer simulations of turbulent flow in a rod-roughened channel, both walls are roughened by equally spaced transverse square rods. The time and spanwise-averaged mean velocity field and turbulence statistics are therefore symmetric about the channel mid-plane in the present flow configuration, whereas highly asymmetric mean velocity profiles are observed in channels with one rough and one smooth wall. A pitch-to-height ratio of 8, i.e. the so-called k-type roughness, is chosen in order to explore a configuration in which the roughness is known to have the largest influence on the mean flow field. The same or similar pitch-to-height ratio has recently been considered by others, e.g. Leonardi et al. (2003a,b). However, the height k of the square rods in the present study is only 1.7% of the channel height, which is smaller by a factor of 3 than in all earlier computer simulations. The height of the roughness elements in wall units is only 13.6. According to the prevailing engineering vocabulary, the present configuration is neither hydrodynamically

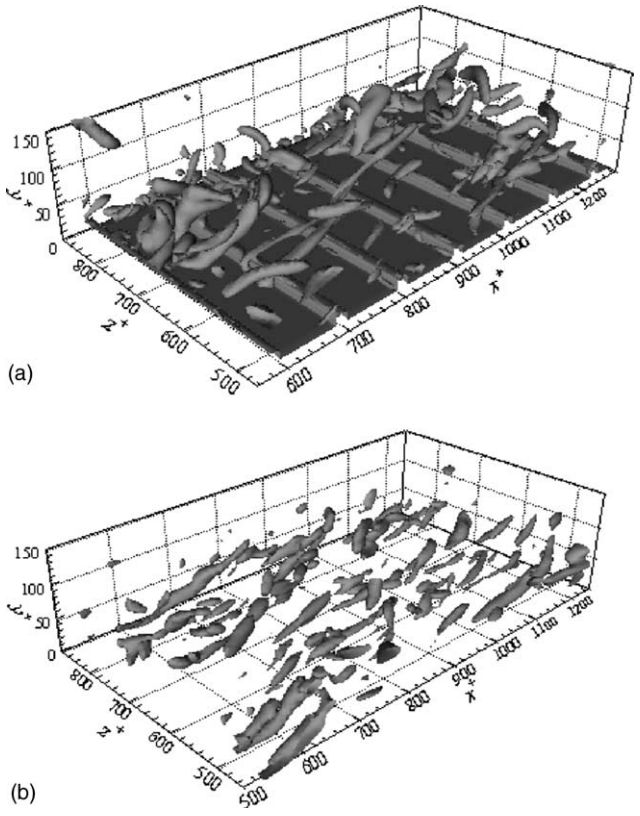

Fig. 14. 3-D Instantaneous vortical structures: (a) rough-wall channel and (b) smooth-wall channel.

smooth nor rough but in the transitional regime where both Reynolds number and relative roughness height matters. The actual computational domain comprised 24 equally spaced square rods on each channel wall and some 19 million grid points were required to assure an adequate resolution.

The Reynolds-averaged streamline pattern exhibits two co-rotating vortices which fill the cavity between two consecutive rods. The averaged flow field which separate from one rod does not reattach and a return flow can be observed all along the bottom of the cavity. The presence of the rods induces substantial changes in the flow field not only within the cavities formed by the gap between two consecutive rods, but also in a certain layer above the crest of the rods. The fairly large extent of the roughness effects is believed to arise from the occasionally vigorous fluid motion originating from the cavities. The associated augmentation of wall-normal momentum exchange is characteristic for k-type roughness. Outside the roughness sublayer, the streamlines become practically parallel with the wall and no discernible streamwise variation of the second-order turbulence statistics can be observed. However, the roughness-induced vertical mean motion $\langle V\rangle$, which enhances the cross-sectional mixing, persists even beyond the roughness sublayer. The dynamical significance of the associated shear $-\langle U\rangle\langle V\rangle$ is negligible compared to the Reynolds shear stress $-\langle uv\rangle$ beyond $5k$. The roughness function ΔU^+, i.e. the characteristic downward shift of the logarithmic part of the mean velocity profile, is found to be 7 and thus significantly below the logarithmic dependency of ΔU^+ on k^+ deduced in the experimental study of Bakken and Krogstad (2003). This observation suggests that the directly simulated flow field is transitionally rough.

Although the mean flow and the turbulence statistics are dramatically affected by the rods within the roughness sublayer, elongated streamwise streaky structures can be observed above the rods. Such streaky structures have not been reported in any of the earlier computational studies of rod-roughened channel flow. The presence of streamwise-oriented streaks is another indication that the flow is in the transitionally rough regime. Since the streaky structures are typically embedded in the buffer region and the innermost part of the logarithmic layer, it is intuitively clear that sufficiently high roughness elements may prevent the formation of conventional wall-layer streaks. The low value of k^+ in the present study explains why the present flow is rather different from that observed by Leonardi et al. (2003a,b) in spite of the same pitch-to-height ratio. This is yet another manifestation that, at least for k-type roughness, both the height of the roughness elements and the spacing between them are crucial parameters.

Acknowledgements

The first author gratefully acknowledges The Research Council of Norway for granting a research fellowship. The research work reported herein has also received support from The Research Council of Norway (Programme for Super-computing) through a grant of computing time. Additional computing time was provided by NTNU's Committee for Computational Scientific Research and Education (BFU). The computer code MGLET was kindly made available by Professor R. Friedrich (TU München) and Professor H. Wengle (Universität Bundeswehr München). The authors are thankful to Professor P.-Å. Krogstad (NTNU Trondheim) for inspiring discussions throughout the course of this study. The valuable comments of the anonymous reviewers helped to improve the quality of the final version of the paper.

References

Antonia, R.A., Krogstad, P.-Å., 2001. Turbulence structure in boundary layers over different types of surface roughness. Fluid Dynam. Res. 28, 139–157.

Bakken, O.M., Krogstad, P.-Å., 2003. Stress measurements in a rough wall channel flow using a variable angle method of calibration for

X-probes. In: Kasagi, N., Eaton, J.K., Friedrich, R., Humphrey, J.A.C., Leschziner, M.A., Miyauchi, T. (Eds.), Proceedings of the Third International Symposium on Turbulence and Shear Flow Phenomena, pp. 105–110.

Bandyopadhyay, P.R., 1987. Rough-wall turbulent boundary layers in the transition regime. J. Fluid Mech. 180, 231–266.

Bergstrom, D.J., Kotey, N.A., Tachie, M.F., 2002. The effects of surface roughness on the mean velocity profile in a turbulent boundary layer. ASME J. Fluids Eng. 124, 664–670.

Cherukat, P., Na, Y., Hanratty, T.J., McLaughlin, J.B., 1998. Direct numerical simulation of a fully developed turbulent flow over a wavy wall. Theor. Comput. Fluid Dynam. 11, 109–134.

Cui, J., Patel, V.C., Lin, C.-L., 2003. Large-eddy simulation of turbulent flow in a channel with rib roughness. Int. J. Heat Fluid Flow 24, 372–388.

De Angelis, V., Lombardi, P., Banerjee, S., 1997. Direct numerical simulation of turbulent flow over a wavy wall. Phys. Fluids 9, 2429–2442.

Djenidi, L., Elavarasan, R., Antonia, R.A., 1999. The turbulent boundary layer over transverse square cavities. J. Fluid Mech. 395, 271–294.

Furuya, Y., Miyata, M., Fujita, H., 1976. Turbulent boundary layer and flow resistance on plates roughened by wires. ASME J. Fluids Eng. 98, 635–644.

George, W.K., Castillo, L., 1997. Zero pressure-gradient turbulent boundary layer. Appl. Mech. Rev. 50, 689–729.

Grass, A.J., Stuart, R.J., Mansour-Tehrani, M., 1993. Common vortical structure of turbulent flows over smooth and rough boundaries. AIAA J. 31, 837–847.

Henn, D.S., Sykes, R.I., 1999. Large-eddy simulation of flow over wavy surfaces. J. Fluid Mech. 383, 75–112.

Ikeda, T., Durbin P.A., 2002. Direct simulations of a rough-wall channel flow. Report No. TF-81, Flow Physics and Computation Division, Department of Mechanical Engineering, Stanford University, Stanford, CA, USA.

Jeong, J., Hussain, F., 1995. On the identification of a vortex. J. Fluid Mech. 285, 69–94.

Kline, S.J., Robinson, S.K., 1990. Quasi-coherent structures in the turbulent boundary layer. Part 1: status report on a community-wide summary of the data. In: Kline, S.J., Afgan, N.H. (Eds.), Near-wall Turbulence. Hemisphere, New York, pp. 200–217.

Krogstad, P.-Å., Antonia, R.A., Browne, L.W.B., 1992. Comparison between rough- and smooth-wall turbulent boundary layers. J. Fluid Mech. 245, 599–617.

Krogstad, P.-Å., Antonia, R.A., 1999. Surface roughness effects in turbulent boundary layers. Exp. Fluids 27, 450–460.

Leonardi, S., Orlandi, P., Djenidi, L., Antonia, R.A., 2003a. Structure of turbulent channel flow with square bars on one wall. In: Kasagi, N., Eaton, J.K., Friedrich. R., Humphrey, J.A.C., Leschziner, M.A., Miyauchi, T. (Eds.), Proceedings of the Third International Symposium on Turbulence and Shear Flow Phenomena, pp. 123–128.

Leonardi, S., Orlandi, P., Smalley, R.J., Djenidi, L., Antonia, R.A., 2003b. Direct numerical simulations of turbulent channel flow with transverse square bars on one wall. J. Fluid Mech. 491, 229–238.

Ligrani, P.M., Moffat, R.J., 1986. Structure of transitionally rough and fully rough turbulent boundary layers. J. Fluid Mech. 162, 69–98.

Maass, C., Schumann, U., 1994. Numerical simulation of turbulent flow over a wavy boundary. In: Proceedings of the First ERCOFTAC Workshop on Direct and Large-Eddy Simulation. Kluwer Academic Publishers, Dordrecht, pp. 287–297.

Manhart, M., 2004. A zonal grid algorithm for DNS of turbulent boundary layers. Comput. Fluids 33, 435–461.

Manhart, M., Friedrich, R., 2002. DNS of a turbulent boundary layer with separation. Int. J. Heat Fluid Flow 23, 572–581.

Manhart, M., Deng, G.B., Hüttl, T.J., Tremblay, F., Segal, A., Friedrich, R., Piquet, J., Wesseling, P., 1998. The minimal turbulent flow unit as a test case for three different computer codes. In: Hirschel, E.H. (Ed.), Notes on Numerical Fluid Mechanics, vol. 66. Vieweg-Verlag, Braunschweig.

Manhart, M., Tremblay, F., Friedrich, R., 2001. MGLET: a parallel code for efficient DNS and LES of complex geometries. In: Parallel Computational Fluid Dynamics – Trends and Applications. Elsevier Science, Amsterdam. pp. 449–456.

Miyake, Y., Tsujimoto, K., Agata, Y., 2000. A DNS of a turbulent flow in a rough-wall channel using roughness elements model. JSME Int. J. 43, 233–242.

Miyake, Y., Tsujimoto, K., Nakaji, M., 2001. Direct numerical simulation of rough-wall heat transfer in a turbulent channel flow. Int. J. Heat Fluid Flow 22, 237–244.

Moser, R., Kim, J., Mansour, N., 1999. Direct numerical simulation of channel flow up to $Re_\tau = 590$. Phys. Fluids 11, 943–945.

Nagano, Y., Hattori, H., Yasui, S., Houra, T., 2003. DNS of velocity and thermal fields in turbulent channel flow with transverse-rib roughness. In: Kasagi, N., Eaton, J.K., Friedrich, R., Humphrey, J.A.C., Leschziner, M.A., Miyauchi, T. (Eds.), Proceedings of the Third International Symposium on Turbulence and Shear Flow Phenomena, pp. 1055–1060.

Perry, A.E., Schofield, W.H., Joubert, P.N., 1969. Rough wall turbulent boundary layers. J. Fluid Mech. 37, 383–413.

Raupach, M.R., Antonia, R.A., Rajagopalan, S., 1991. Rough-wall turbulent boundary layers. Appl. Mech. Rev. 44, 1–25.

Schumann, U., 1975. Subgrid scale model for finite difference simulations of turbulent flows in plane channels and annuli. J. Comp. Phys. 18, 376–404.

Townsend, A.A., 1976. The Structure of Turbulent Shear Flow, 2nd ed. Cambridge University Press.

Tsujimoto, K., Miyake, Y., Nagai, N., 2001. Direct numerical simulation of turbulent mixing in a rough-wall flow. In: Liu, C., Sakkel, L., Beutner, Th. (Eds.), DNS/LES Progress and Challenges. Greyden Press. pp. 541–548.

Werner, H., Wengle, H., 1993. Large-eddy simulation of turbulent flow over and around a cube in a plane channel. In: Durst, F. et al. (Ed.),. In: Turbulent Shear Flows, 8. Springer-Verlag, Berlin, pp. 155–168.

Wood, D.H., Antonia, R.A., 1975. Measurements in a turbulent boundary layer over a d-type surface roughness. ASME J. Appl. Mech. 42, 591–597.